Supplement of Atmos. Chem. Phys., 21, 10375–10391, 2021
https://doi.org/10.5194/acp-21-10375-2021-supplement


Atmospheric Chemistry and Physics
Open Access

*Supplement of*

# Contrasting effects of secondary organic aerosol formations on organic aerosol hygroscopicity

**Ye Kuang et al.**

*Correspondence to:* Shan Huang (shanhuang_eci@jnu.edu.cn) and Min Shao (mshao@pku.edu.cn)

## 1. Site map

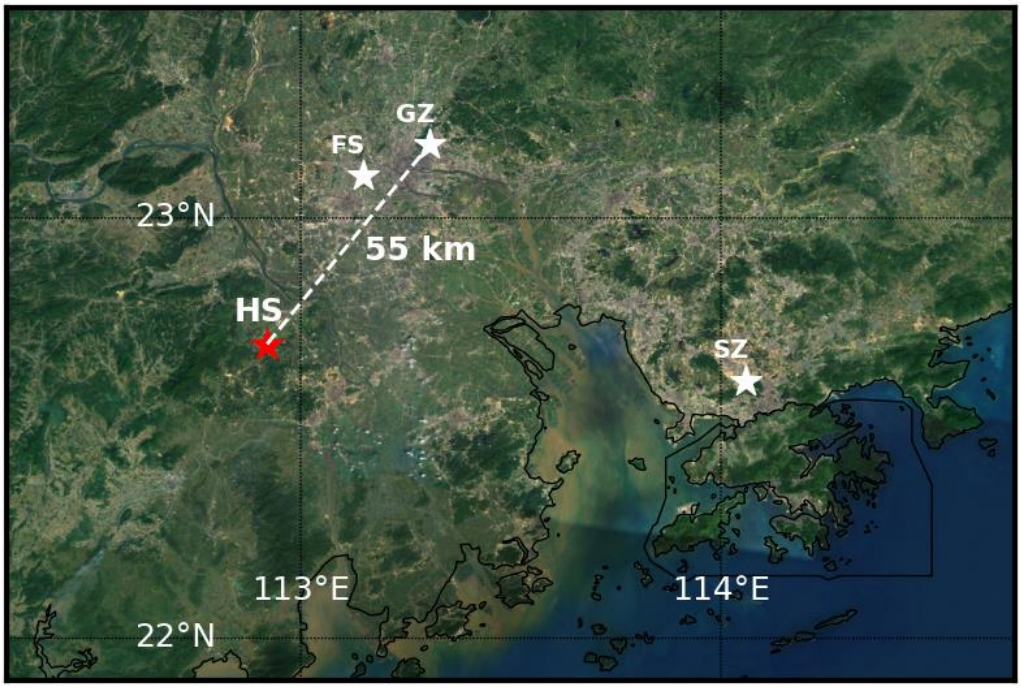


Figure S1. Locations of Heshan (HS) site, and other mega cities (FS:Foshan, GZ:Guangzhou, SZ:Shenzhen) in the Pearl river delta region (map background obtained through python from http://server.arcgisonline.com/ArcGIS/rest/services/ESRI_Imagery_World_2D/MapServer/, Copyright:© 2013 ESRI, i-cubed, GeoEye).

## 2. Details on quantifying uncertainties of using $\kappa_{f(\mathrm{RH}),PM_{10}}$ represent $\kappa_{chem,PM_1}$

In Eq.3, other than aerosol composition measurements, what's the accuracy of using $\kappa_{f(\mathrm{RH}),PM_{10}}$ represent $\kappa_{chem,PM_1}$ need to be carefully quantified. As discussed in Kuang et al. (2020), the difference between $\kappa_{chem,PM_1}$ and $\kappa_{f(\mathrm{RH}),PM_{10}}$ are both influenced by aerosol PNSD and size-resolved κ distribution. To cover as many cases as possible, we have performed a simulation to investigate the relative differences between $\kappa_{chem,PM_1}$ and $\kappa_{f(\mathrm{RH}),PM_{10}}$ under different conditions of aerosol chemical compositions through varying size distributions of ammonium nitrate, ammonium sulfate, organic aerosol, dust and BC, and their mass fractions randomly, and the mass size distributions follow lognormal distributions, that is:

$$\mathrm{dM/dlogDp} = \frac{\mathrm{Mtot*fx}}{\sqrt{2\pi}\log(\sigma_{\mathrm{g,x}})}\exp\left[-\frac{(\log(\mathrm{D}_p)-\log(\mathrm{D}_{\mathrm{g,x}}))^2}{2\log^2\sigma_{\mathrm{g,x}}}\right], \qquad \text{Eq. 1}$$

where x corresponding different aerosol compositions, and fx corresponding to its mass fractions. The parameters used in simulations are listed in Table S1, the number of randomly produced datasets for simulating $\kappa_{chem,PM_1}$ and $\kappa_{f(\mathrm{RH}),PM_{10}}$ is 10000.

Table S1. used parameters for simulating differences between $\kappa_{chem,PM_1}$ and $\kappa_{f(\mathrm{RH}),PM_{10}}$, m and σ corresponds to average and standard deviation respectively.

| | fx range (%) | $D_g$ (nm) | | $\sigma_g$ | | $\rho$ | | κ | |
|---|---|---|---|---|---|---|---|---|---|
| | | m | σ | m | σ | m | σ | m | σ |
| Ammonium Nitrate | 0-50 | 450 | 100 | 2.2 | 0.25 | 1.72 | | 0.56 | |
| Ammonium sulfate | 0-50 | 550 | 100 | 2.2 | 0.25 | 1.78 | | 0.56 | |
| Organic Aerosol | 10-60 | 450 | 150 | 2.2 | 0.25 | 1.2 | 0.05 | 0.15 | 0.05 |
| Dust | 5-50 | 2500 | 500 | 2.2 | 0.25 | 2 | | 0.05 | 0.015 |
| BC | 0-12 | 250 | 100 | 2.2 | 0.25 | 1.7 | | 0 | |

## 3. Analysis on possible pathways of nitrate increase

Depending on the RH or the RH history that aerosol particles have been experienced, the aerosol particles might be solid (if crystallized) or aqueous phase (dehydration branch from the morning to the afternoon, metastable) after about 16:00. However, when aerosol particles will be deliquescent is also a puzzle if aerosol particle crystallized in the afternoon due to the complex dependence of deliquescence RH on aerosol mixtures of ammonium sulfate, ammonium nitrate and organic aerosols (Kuang et al., 2016), and the peak RH in the morning was usually lower than 80%. To illustrate the possible mechanisms behind the nitrate increase, we assume the following two states of ammonium nitrate: (1) solid state; (2) aqueous phase.

For the solid phase case, the $NH_3(g) + HNO_3(g) \leftrightarrow NH_4NO_3(s)$ equilibrium theory is applied (reference). If we have the initial concentration of gaseous $NH_3$, then we can guess the initial $HNO_3$ (g) based on the $K_p(T)$ and estimate the nitrate concentration increase due to the decrease $K_p(T)$, the $K_p(T)$ changed from 84 $ppb^2$ to 24 $ppb^2$ from 16:30 to 23:30 for the average case with air temperature decrease from 27.7 to 22.7 °

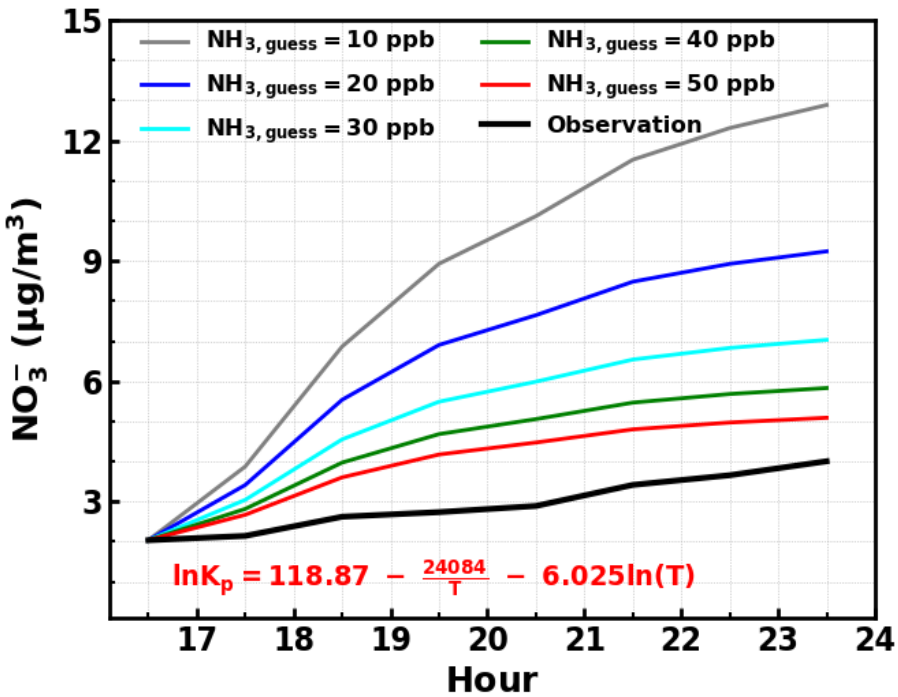


**Figure S2**. Simulated variations of nitrate under different NH3 (g) conditions by assuming aerosol particles are solid and using the Kp(T) theory.

C. Figure S2 shows the variations of nitrate mass concentrations under different assumed $NH_3$ (g) concentration conditions by considering variations of $K_p(T)$. The results demonstrate that the temperature induced $K_p(T)$ change is enough for explaining observed nitrate increase, and thus a possible mechanism.

For the aqueous phase case, $NH_4NO_3$ will be found in the aqueous state, and the corresponding dissociation reaction is then $NH_3(g) + HNO_3(g) \leftrightarrow NH_4^+ + NO_3^-$. For

this case, both temperature decrease and RH increase play roles in the $NH_3$ and $HNO_3$ partitioning. We use a thermodynamic model ISORROPIA (forward, metastable) to simulate the possible magnitude of nitrate increase driven by increased RH and reduced temperature for the average case shown in Fig.3 of the manuscript. We also assume different scenarios of $NH_3$(g) concentrations and for each $NH_3$(g) concentration scenario, we estimate the $HNO_3$(g） concentration with which we can reproduce the observed nitrate concentration at the initial time (16:30), to get a total $HNO_3$ concentration in gas and aerosol phase, then we can estimate the possible increase of nitrate in aerosol phase due to repartitioning and the results are shown in Figure S3. The results show that the more $HNO_3$ dissolved in aqueous phase can also explain the observed nitrate mass concentration increase.

The simulation results shown above demonstrate that repartitioning of $HNO_3$ (total $HNO_3$ in aerosol and gas phase remain unchanged) can explain the observed nitrate concentration increase under both assumptions that aerosols are completely aqueous or sold. The actual atmospheric case is more likely that both solid (freshly emitted and crystallized) and aqueous particles (dehydration branch, not crystallized) exist, however, does not affect conclusion that the repartitioning of $HNO_3$ in gas and aerosol phase can explain the observed nitrate increase. In addition, NO concentration is quite low after 16:00 which might be favorable of $N_2O_5$ formation and the $N_2O_5$ hydrolysis as a possible nitrate formation pathway cannot be excluded.

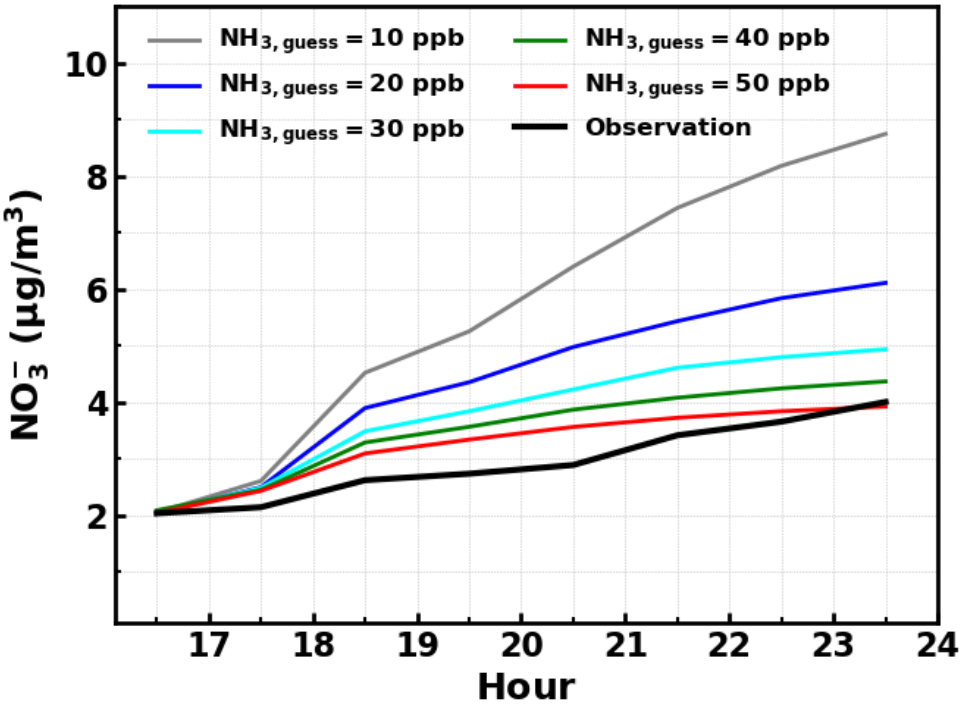


**Figure S3**. Simulated variations of nitrate under different NH3 (g) conditions by assuming aerosol particles are aqueous using the ISORROPA thermodynamic model.

## 4. Supplementary figures

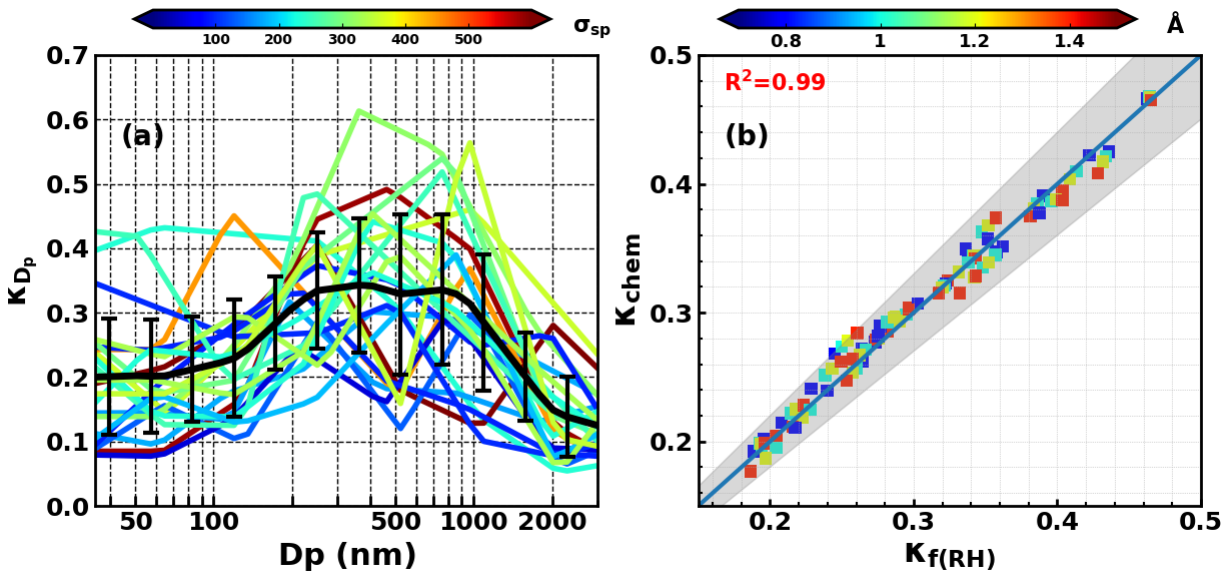


Figure S4. (a) Size-resolved $\kappa$ distributions which are derived from measured size-segregated chemical compositions during HaChi campaign, colors represent corresponding values of average $\sigma_{sp}$ at 550 nm ($Mm^{-1}$), black solid line is the average size-resolved $\kappa$ distribution and error bars are standard deviations. (reprint from (Kuang et al., 2018)); (b) Comparison of simulated $\kappa_{f(\mathrm{RH})}$ of PM10 and $\kappa_{chem}$ of PM1

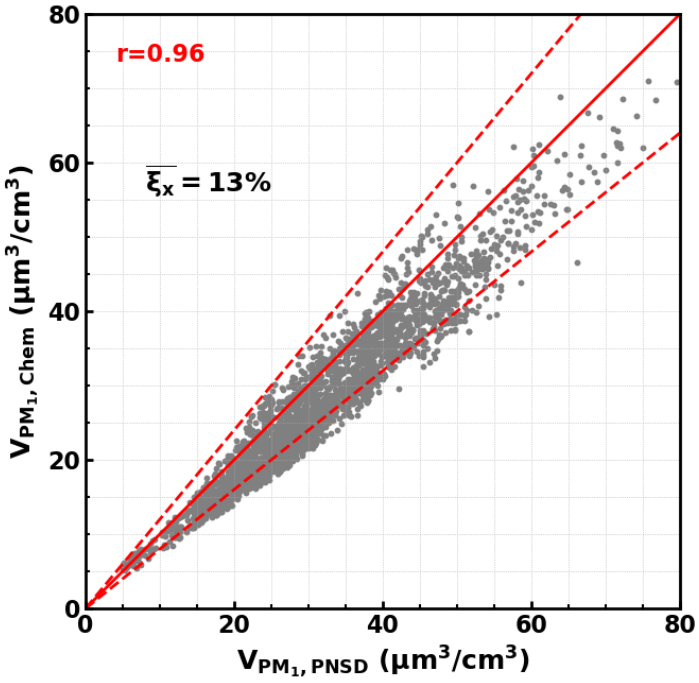


**Figure S5**. Comparison between $PM_1$ volume concentration derived from SMPS (x-axis) and SP-AMS (y-axis) measurements. Dashed red lines represent 20% relative difference lines.

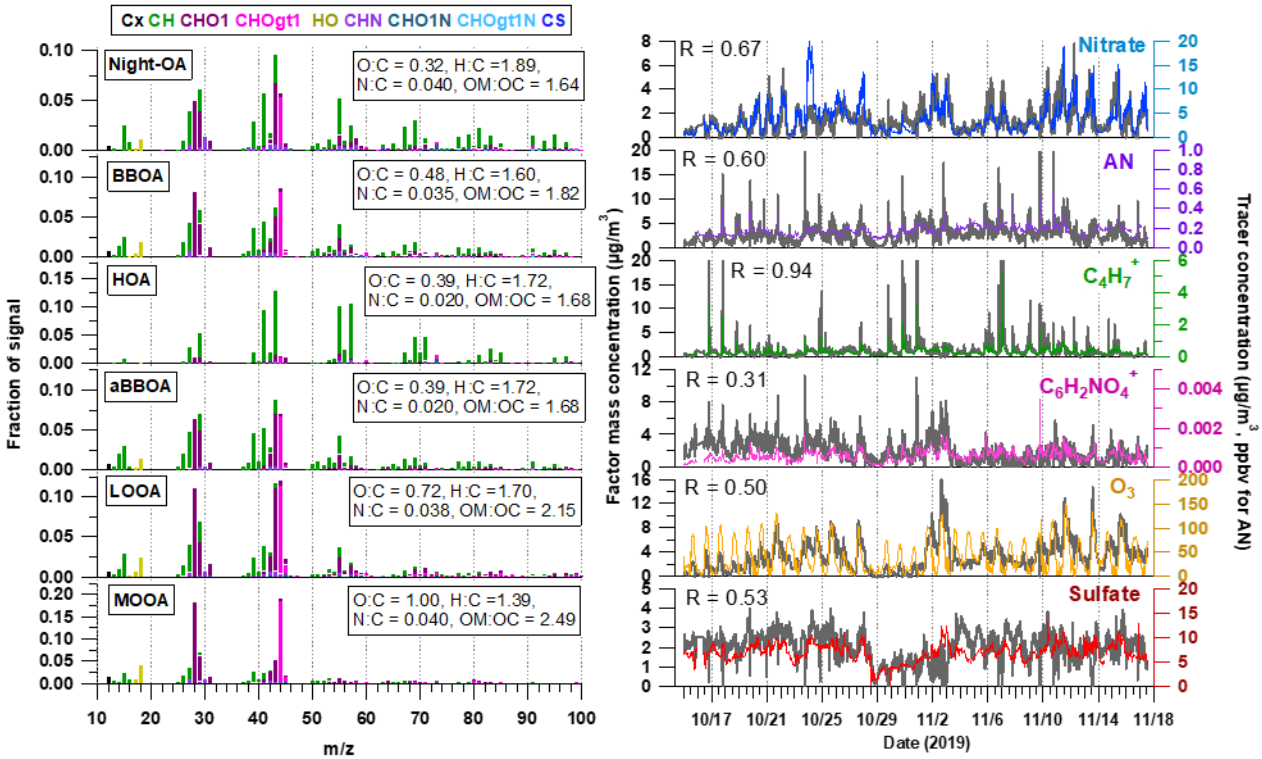


**Figure S6**. **(a)** Mass spectral profile in family groups and **(b)** time series of PMF OA components. Also exhibited are concentration variations of tracer compounds on the right axes.

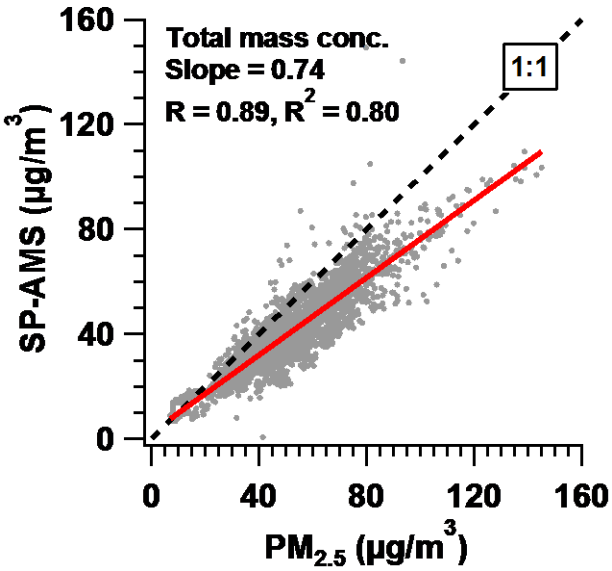


**Figure S7**. Comparison between $PM_{2.5}$ mass concentration provided by local authority and total mass concentration measured by SP-AMS.

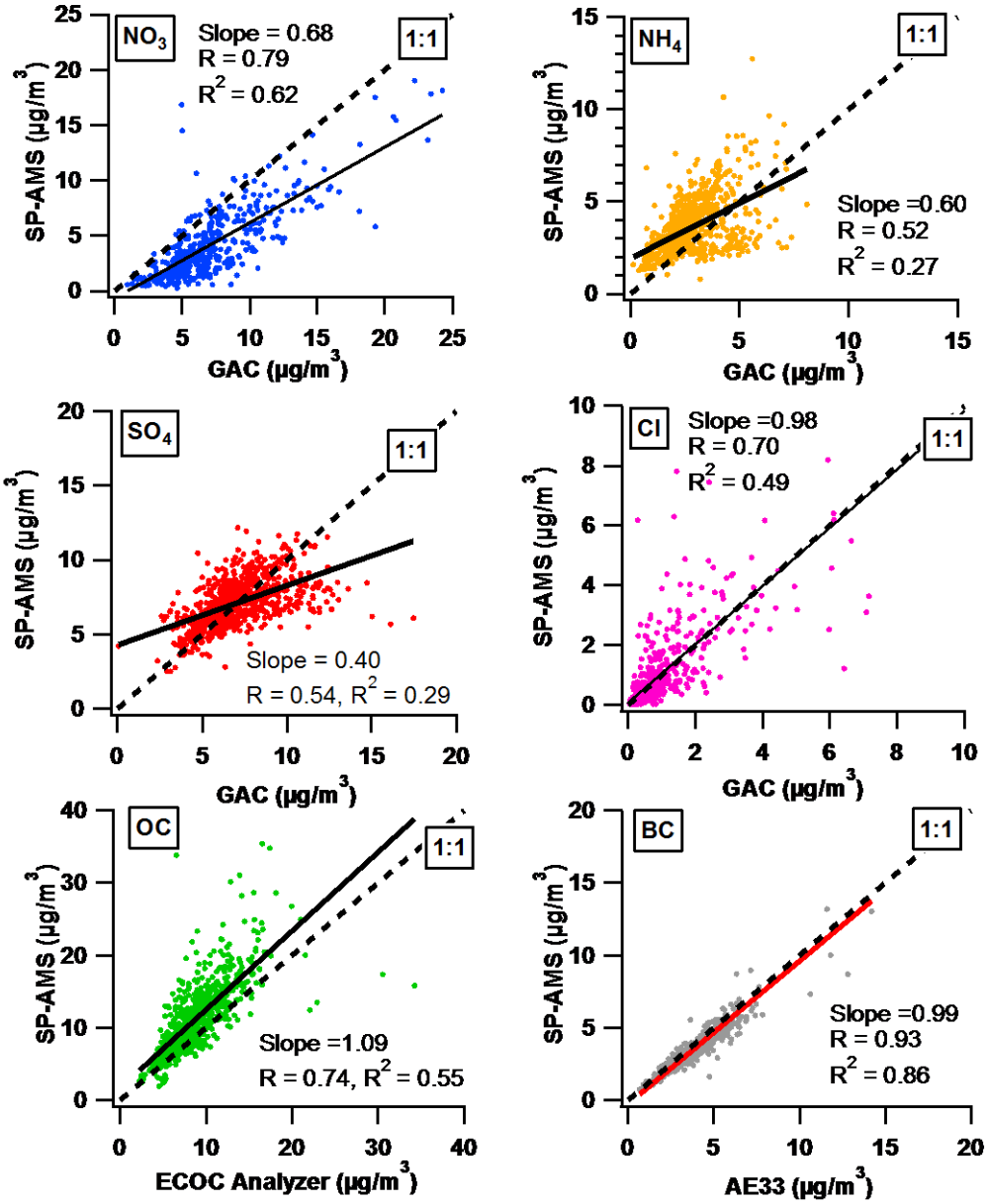


**Figure S8**. Comparisons of aerosol compositions between SP-AMS (PM1) and external online measurements, including gas aerosol collection system (GAC) with ion chromatography (with PM2.5 impactor), ECOC Analyzer (Sunset, xxx, Inc) and AE33 aethalometer. Note that organic carbon (OC) was calculated by organics from SP-AMS divided ratio of OM and OC provided by AMS HR data, and then compared with OC derived from ECOC analyzer.

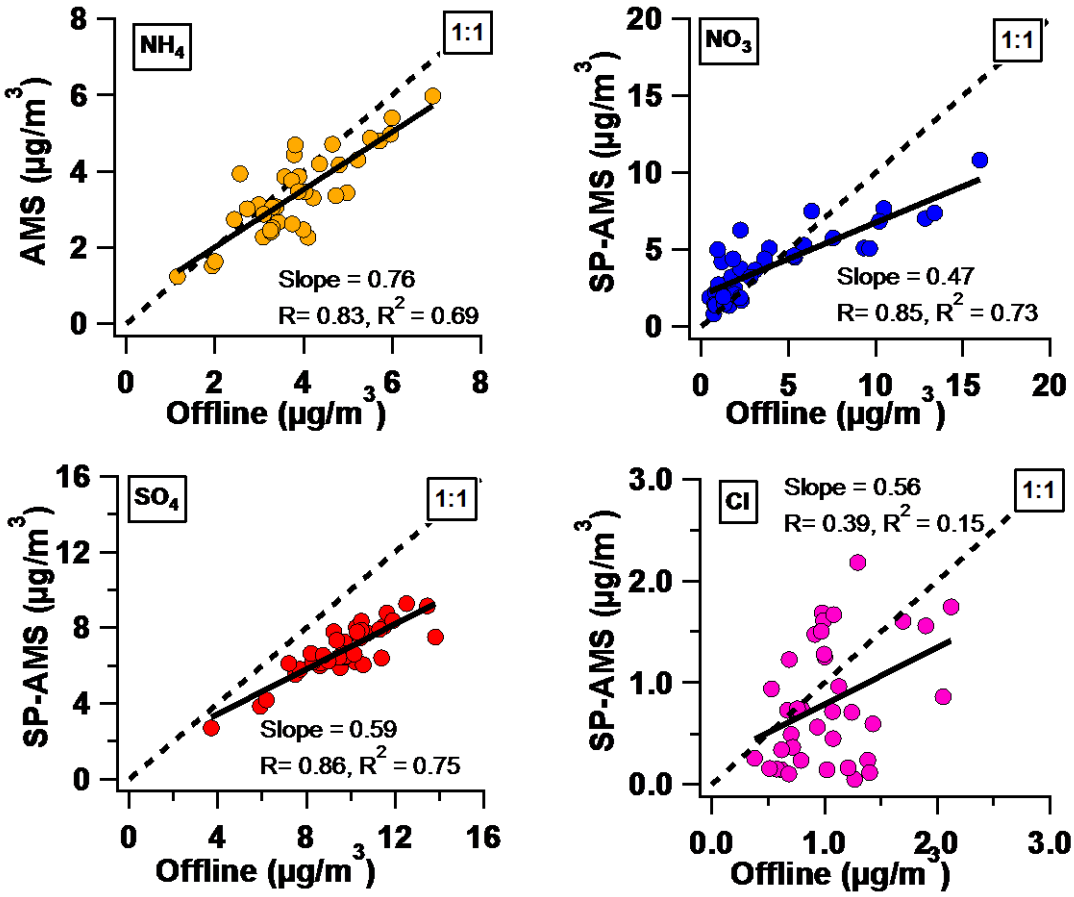


**Figure S9**. Comparisons of ammonium, nitrate, sulfate and chloride between SP-AMS (PM1) and offline measurements with PM2.5 impactor.

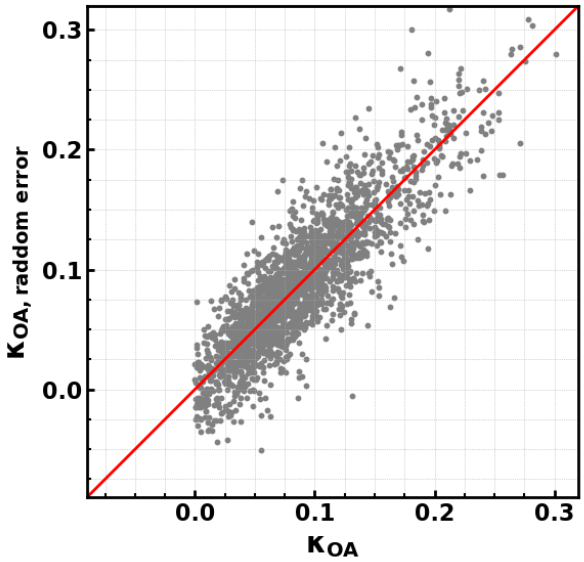


**Figure S10**. Comparison between $\kappa_{OA}$ derived with and without random errors

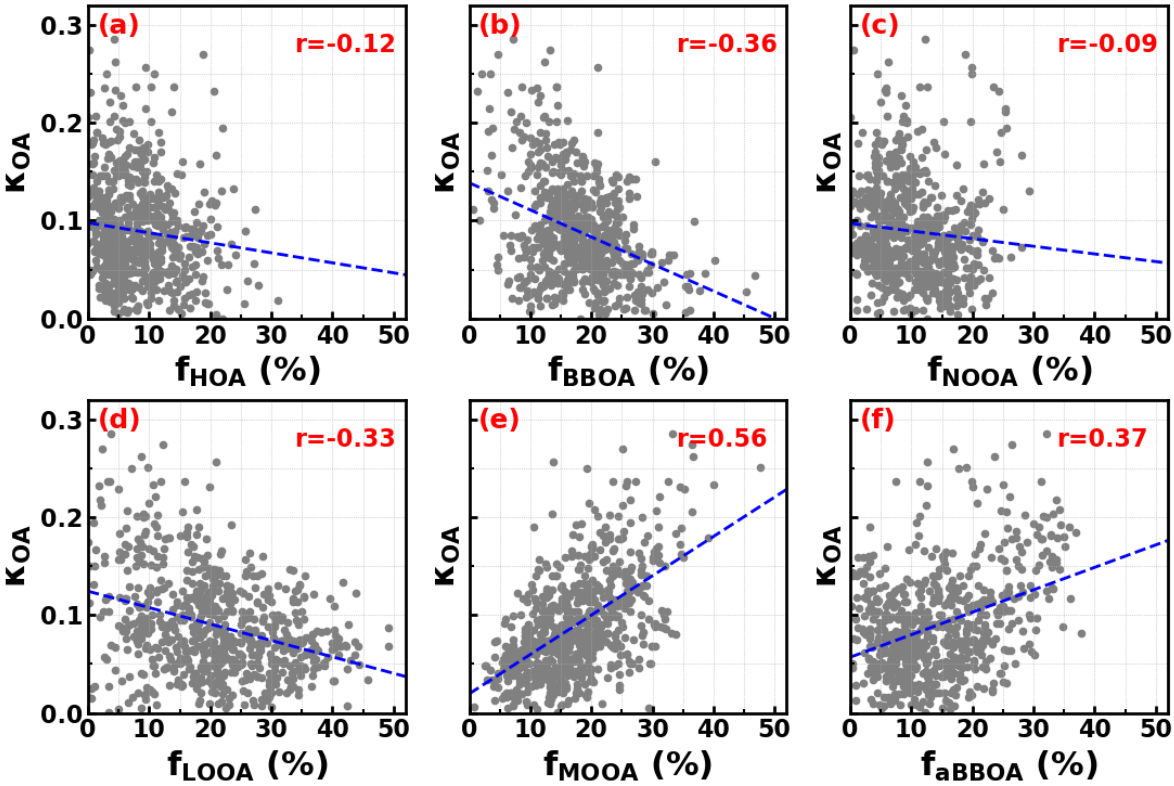


**Figure S11**. Correlations between $\kappa_{OA}$ derived with random errors and mass fractions of OA factors in total OA mass

Kuang, Y., Zhao, C. S., Ma, N., Liu, H. J., Bian, Y. X., Tao, J. C., and Hu, M.: Deliquescent phenomena of ambient aerosols on the North China Plain, Geophysical Research Letters, n/a-n/a, 10.1002/2016GL070273, 2016.

Kuang, Y., Zhao, C. S., Zhao, G., Tao, J. C., Xu, W., Ma, N., and Bian, Y. X.: A novel method for calculating ambient aerosol liquid water content based on measurements of a humidified nephelometer system, Atmospheric Measurement Techniques, 11, 2967-2982, 10.5194/amt-11-2967-2018, 2018.

Kuang, Y., He, Y., Xu, W., Zhao, P., Cheng, Y., Zhao, G., Tao, J., Ma, N., Su, H., Zhang, Y., Sun, J., Cheng, P., Yang, W., Zhang, S., Wu, C., Sun, Y., and Zhao, C.: Distinct diurnal variation in organic aerosol hygroscopicity and its relationship with oxygenated organic aerosol, Atmos. Chem. Phys., 20, 865-880, 10.5194/acp-20-865-2020, 2020.